

## 中文摘要

本研究利用真空液壓壓鑄製程，結合 20 nm、70 nm 與 220 nm 管胞孔徑的陽極氧化鋁模板(Anodic Aluminum Oxide, AAO)技術，成功地製造出錫鈹共晶 (Bi-43 wt % Sn) 奈米線。有別於錫鈹塊材的層狀共晶結構，錫鈹共晶奈米線則是沿著線軸，呈現錫與鈹元素交替分佈的段狀共晶結構；在各個組成區段中，各元素均為單晶結構。比較不同管徑之錫鈹共晶奈米線之後，較細之奈米線傾向有較長的析出區段。而且，在單一線材中，錫與鈹區段的長度比例會接近 3.3 : 1。本製程的特色，不同於一般需要將材料離子或分子化的沉積製程；將合成好之材料加熱溶解，直接注入氧化鋁奈米孔洞，凝固後即成為一維奈米材料，可精準的控制並維持塊材所配置之材料成分配比。

參考固化理論，提出段狀結構之形成機制，並結合電子顯微鏡臨場觀察奈米線材之退火過程，詳細說明奈米線材微結構與凝固冷卻型態之關係。沿著線軸的方向性冷卻行為，促使共晶奈米線也沿著線軸的方向交替析出。在重新溶解凝固的退火實驗中，比較 70 nm 與 200 nm 的線材，較大的管徑有利於流體的對流行為；因此，在相同退火條件下，尺寸效應造成凝固行為的差異，細管徑將限制融熔金屬的流動行為，使得固化之後的微結構產生變化。真空壓鑄冷卻過程是有方向性的，將會有利於段狀的共晶結構線材形成；相對地，退火過程則是等向性冷卻，有利於整體均勻分布的多晶結構。

最後，利用本方法所獲得的錫鈹共晶奈米線，直接於空氣爐中高溫退火，便可進一步地獲得氧化鈹-氧化錫( $\text{BiO}_x\text{-SnO}_x$ )之複合奈米線材。將奈米線材由氧化鋁模板中溶出時，蝕刻液會在合金線表面造成氧化，此自然生成的氧化層即可與內部合金形成同軸管(core-shell)結構，並可防止內部合金在高溫製程中的流失。當此同軸管奈米線在空氣爐中，以每分鐘 50°C 的升溫速率加熱至 700 °C；經歷持溫一個小時的退火處理後，便可直接獲得所稱之複合氧化物線材。進一步分析氧化物之光學性質，陰極發光(Cathodoluminescence, CL)光譜與光導效應(Photoresponse)光譜也同時用以佐證氧化鈹與氧化錫的存在。

關鍵字：錫鈹共晶奈米線、固化過程、尺寸效應、氧化鈹-氧化錫之複合奈米線材



# Abstract

Eutectic Bi-43Sn (in weight percent) nanowires with diameters of 20 nm, 70 nm and 220 nm respectively, were fabricated by a vacuum hydraulic pressure injection process using anodic aluminum oxide (AAO) as templates. Novel eutectic microstructure was found within the fabricated nanowires, which composed of alternating Bi and Sn segments along their wire axes. Within the segments, the electron diffraction analysis revealed single crystalline structures of Bi and Sn elements respectively. Parameters that control the nanowire fabrication process were discussed. It was found that as the wire diameter reduced, longer Bi and Sn segments formed. In addition, the alternative segmental compositions showed that the ratio of tin to bismuth is approximately 3.3:1. For this process, nanowires were formed from non-ion deposition with liquid alloy; in this way, the composition of nanowires can be controlled precisely in stoichiometry.

The size effects on solidification and the formation mechanism of the segmented eutectic Bi-43Sn nanowires have also been investigated during the in situ reheating processes. A directional solidification along the wire axis limits the segmented eutectic nanowire to arrange axially due to directional solidification and the sequential enrichment of two elements. In 70 nm nanowires, the small size confines the convection in liquid, which results in differences in the microstructure and composition profiles between 70 and 200 nm nanowires during the reheating process. In the vacuum hydraulic pressure injection process, the directional cooling helps the formation of single crystal, and the isotropic solidification leads to polycrystalline microstructure.

Finally, bismuth oxide-tin oxide ( $\text{BiO}_x\text{-SnO}_x$ ) heterostructure nanowires with a diameter of 70 nm were fabricated by directly annealing Bi-Sn eutectic nanowires. After removal of AAO template with etching solution, a spontaneous oxide was formed on the nanowires,

enclosing the Bi-Sn eutectic alloys. While these nanowires went through the annealing process at a heating rate of 50 °C/ min, the well-annealed oxide nanowires remained solid, straight and segmental. The results of cathodoluminescence (CL) spectrum and photoresponse proved that the products comprised bismuth oxide and tin oxide. This fabrication methodology is a simple way to fabricate one-dimensional oxide nanomaterials.

*Keywords: Bi-Sn eutectic nanowires, Solidification, Size Effect, BiOx-SnOx nanowires*



## 致 謝

這漫長學習過程，最感謝的是給予我最多指導與協助的陳建仲教授。從一踏入研究的領域，總是你不厭其煩的教導與叮嚀；不論是在生活、工作或課業上，總是把你的經驗跟我分享，讓我少走很多冤枉路，也一起度過許多歡笑與煎熬的歲月；許多個熬夜的實驗日子，你也總是用驚人的意志力告訴我，人生態度就是要堅持下去，用心投入於你所選擇的事情；如今，總算到了一個豐收的季節，將這獲得的成果與你分享，希望往後每個收穫的日子，能一直分享於你。

感謝朱英豪教授，在我遇到最大的瓶頸時，你剛好歸國服務；引薦我認識吳文偉教授，讓我的問題找到最適當的解決方法。在研究的閒暇之餘，你還要忍受我跟你不斷地抱怨與閒聊，但你總是很樂意聽我的廢話，更以學長的身分跟我經驗分享，讓我體會到默默做大事的人的氣度。在此，還是要向你表示我心裡由衷的感謝。

感謝清大的王秋燕博士。與你的合作相當的順利且有效率，從你身上我學到做事的積極與認真；跟你合作之後，讓我也不由自主的跟著積極起來，讓這最後收尾的腳步加快不少。感謝同實驗室的永昌學弟，每次打電話給你，你總是有辦法給我即時的幫助；在這邊希望你可以研究順利，需要幫忙的時候也請別客氣啦。還要感謝清大材料系的彥鈞學弟，陪學長打球打屁吃吃喝喝，也祝你研究順利。感謝已經畢業的進興和喬盈，還有仍在交大應化系的慧屏，令我去到應化系，都有種回到自己系上的熱鬧感覺。

感謝大學一直到現在的同學小蛙還有俊元房東，總是收留我在新竹的每一天，陪我放鬆聊天、吃吃喝喝、打電動。有了你們，讓我在新竹不會有流浪的感覺，雖然你們都會問我哪個時候要畢業，問的讓我不知所措，但是我對你們的感激是不會打折的。還有，結完婚就人間蒸發的黑狗，也要謝謝你在流體力學的幫助，也勉強提到你一下吧。

最後，由衷的感謝一直以來最支持我的家人，老爸、老媽、哥嫂、姐。總是讓我沒有後顧之憂的做我想做的事情，我也會盡力做到讓你們不用擔心，總算努力完成，沒有讓你們失望。這個成果與榮耀最有價值的地方就是有你們一路的支持與陪伴，謝謝你們，我最親愛的家人。感謝陪在我身邊，一起成長打氣的女朋友佩娟，對我的包容與溝通，願這輩子都能與你走下去。

# Content

Abstract (Chinese).....	I
Abstract (English) .....	III
Acknowledge .....	V
Content.....	VI
Table Captions.....	IX
Figure Captions.....	X

## Chapter 1 Introduction

1.1 General Background.....	1
1.2 Organization of the Dissertation.....	3
Reference.....	5



## Chapter 2 Literature Review

2.1 Eutectic Bismuth-Tin (Bi-Sn) Alloy.....	7
2.2 Fabrication of Nano-materials by Nonlithographic Methods.....	10
2.3 Vacuum Hydraulic Pressure Injection Process.....	12
2.4 Anodic Aluminum Oxide (AAO).....	17
2.4.1 Introduction to AAO.....	17
2.4.2 Electropolishing of Aluminum.....	17
2.4.3 Anodizing of Aluminum.....	19
2.5 Fluid Mechanics Principles of Melting Alloys within Nanowires.....	23
2.6 Solidification of Eutectic.....	26
2.7 One-Dimensional Bismuth Oxide and Tin Oxide (Bi <sub>2</sub> O <sub>3</sub> -SnO <sub>2</sub> ).....	29

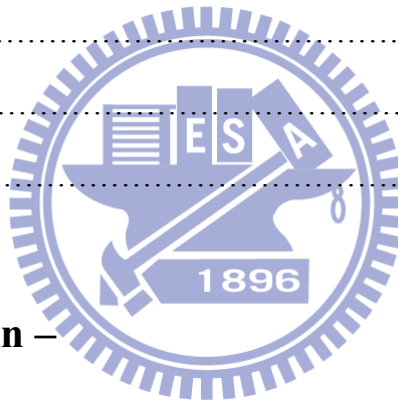
2.7.1 Bismuth Oxide.....	29
2.7.2 Tin Oxide.....	30
Reference.....	32

**PART I: Fabrication –**

**Chapter 3 Fabrication and Characterization of Eutectic**

**Bismuth-Tin (Bi-Sn) Nanowires**

3.1 Backgrounds and Motivation.....	35
3.2 Experimental Procedures.....	36
3.3 Results and Discussion.....	37
3.4 Summary.....	40
Reference.....	41



**PART II: Solidification –**

**Chapter 4 Novel Morphology and Solidification Behavior of**

**Eutectic Bismuth–Tin (Bi–Sn) Nanowires**

4.1 Backgrounds and Motivation.....	53
4.2 Experimental Procedures.....	55
4.3 Results and Discussion.....	56
4.4 Summary.....	58
References.....	59

**Chapter 5 The Size Effect on Solidification in Eutectic**

## **Bismuth–Tin (Bi–Sn) Nanowires by In-Situ Reheating Processes**

5.1	Backgrounds and Motivation.....	66
5.2	Experimental Procedures.....	67
5.3	Results and Discussion.....	68
5.4	Summary.....	72
	Reference.....	74

### **PART III: Application –**

#### **Chapter 6 Fabrication of Bismuth Oxide-Tin Oxide Nanowires**

##### **by the Direct Thermal Oxidation of Bi-Sn Eutectic Nanowires**

6.1	Backgrounds and Motivation.....	87
6.2	Experimental Procedures.....	88
6.3	Results and Discussion.....	88
6.4	Summary.....	90
	Reference.....	92

#### **Chapter 7 Conclusions and Suggestions for Future Work**

7.1	Conclusions.....	98
7.2	Suggestions for Future Work.....	100



## Table Captions

### Chapter 5

Table 5.1 Experimental heating conditions and the results of compositions for eutectic Bi-Sn nanowires.



## Figure Captions

### Chapter 2

Figure 2.1 Phase diagram of Bi-Sn alloy.

Figure 2.2 Microstructure of eutectic Bi-Sn alloy.

Figure 2.3 Schematic apparatus of vacuum hydraulic pressure injection process.

Figure 2.4 SEM image of Sn melt inside AAO, which formed Sn nanowires: (a) top view, (b) cross-section view.

Figure 2.5 The I-V curve of etching, polishing and pitting sections.

Figure 2.6 Schematic image of an ideal ordered anodic porous alumina.

Figure 2.7 Relationship between interpore distances and anodic voltages for AAO forming process in sulfuric acid, oxalic acid, and phosphoric acid, respectively.

Figure 2.8 SEM images of AAO pores with the size of (a) 20 nm, (b) 70 nm, and (c) 220 nm respectively.

Figure 2.9 Illustration of types of flow inside a pipe.

Figure 2.10 Illustration of developing stages of the flow in a pipe.

Figure 2.11 Eutectic point at binary phase diagram.

Figure 2.12 Illustration of eutectic solidification.

Figure 2.13 Typical eutectic microstructures.

Figure 2.14 Transformation temperatures for  $\alpha$ -,  $\beta$ -,  $\gamma$ -,  $\delta$ - and  $\varepsilon$ -Bi<sub>2</sub>O<sub>3</sub>.

### Chapter 3

Figure 3.1 Binary Bi-Sn phase diagram.

Figure 3.2 Characterization of starting material, the Bi-Sn bulk eutectic alloy. (a)

Back-scattered SEM image of lamellar structure; (b) EDS mapping of Bi; (c) EDS

mapping of Sn; (d) XRD spectrum showing purely Bi and Sn peaks; (e) DSC spectrum.

Figure 3.3 SEM images of (a) AAO template with 20 nm pore size, (b) 20 nm Bi-Sn nanowires bundles, and (c) freed 20 nm nanowires.

Figure 3.4 SEM images of (a) AAO template with 70 nm pore size, (b) 70 nm Bi-Sn nanowires bundles, and (c) freed 70 nm nanowires.

Figure 3.5 SEM images of (a) AAO template with 220 nm pore size, (b) 220 nm Bi-Sn nanowires bundles, and (c) freed 220nm nanowires.

Figure 3.6 Calculation of the applied pressure as a function of the pore diameter of AAO for the experimental alloy.

Figure 3.7 TEM image and analyses of the 220 nm Bi-Sn eutectic nanowire.

Figure 3.8 STEM image and the elemental mapping from the framed area of the 220 nm Bi-Sn eutectic nanowire.

Figure 3.9 STEM image and elemental mapping of the 70 nm Bi-Sn eutectic nanowire.

Figure 3.10 STEM image and elemental mapping from the framed area of the 20 nm Bi-Sn eutectic nanowire.

## Chapter 4

Figure 4.1 Solidification of an alloy with equilibrium at the liquid-solid interface. (a) Phase diagram; (b) composition profile across the interface.

Figure 4.2 Composition profile in solidification with limited liquid diffusion and no convection in solid.

Figure 4.3 Typical OM image of casted bulk Bi-Sn eutectic material with a lamellar microstructure.

Figure 4.4 SEM images of fabricated Bi-Sn nanowire bundle and magnified image of a part.

(Insert)

Figure 4.5 High-resolution back-scattered SEM images of Bi-Sn eutectic nanowire (a) a large overview of a nanowire bundle; (b) magnified image showing the banded eutectic structure.

Figure 4.6 STEM image and the element mapping from the framed area of the 220 nm Bi-Sn eutectic nanowires.

Figure 4.7 Example of hypoeutectic, *A*, and hypereutectic, *B*, composition points in a binary Bi-Sn phase diagram.

## Chapter 5

Figure 5.1 Schematic illustration of the solidification processes during the vacuum hydraulic pressure process within AAO membrane: (a) injection of the melted alloy into AAO membrane under steady pressure, (b) complete solidification of the nano-materials, (c) removal the residual alloy.

Figure 5.2 Schematic illustrations of the (a) heating, (b) holding and (c) cooling processes of a 70 nm nanowires within the in situ reheating setup.

Figure 5.3 *In situ* TEM image sequences of the diffusion behavior during the reheating process within 70 nm eutectic Bi-Sn nanowires at (a) room temperature, (b) 80 °C, (c) 138 °C, (d) 150 °C. The bright area is Sn, and the dark area is Bi, and the insets in (b) show the selective area electron diffraction pattern of Bi and Sn segments. The heating rate is 50°C/min.

Figure 5.4 The fine TEM image of 70 nm eutectic Bi-Sn nanowire at 150 °C and the EDS spectrums from two distinct segments.

Figure 5.5 *In situ* TEM image sequences of a 200 nm eutectic Bi-Sn nanowire at (a) room

temperature, (b) 138 °C, (d) 150 °C. The bright area is Sn, and the dark area is Bi.

The heating rate is 50°C/min.

Figure 5.6 Relationship between compositions and temperatures for the individual (a) Bi and (b) Sn segments inside nanowires of both 70 nm and 200 nm during the reheating process.

Figure 5.7 TEM images of the end tip of an individual Bi-Sn nanowire with average diameters of (a) 70 nm and (b) 200 nm. (c) Relationship between compositions and temperatures taken from the arrowed position in (a).

Figure 5.8 Schematic illustrations of the diffusion behaviors in different positions within a single eutectic Bi-Sn nanowire of 70 nm. From top, they present (a) the sketch of a single wire, (b) the diffusion directions within each segment, and (c) the concentration profiles along the wire axis (in weight percentage).

Figure 5.9 TEM image, EDS spectrum, and SAED patterns of a 70 nm Sn-Bi eutectic nanowire with polycrystalline microstructure after *in situ* reheating.

## Chapter 6

Figure 6.1 (a) SEM image of as-injected Bi-Sn eutectic nanowires after removal of AAO template with etching solution. The core-shell of the segmental structure was observed. (b) SEM image of nanowires annealed at an excessive heating rate.

Figure 6.2 TEM images of Bi-Sn eutectic nanowires annealed at (a) an excessive and (b) the proper heating rates. The oxides were not dense enough to confine the melting alloys when the heating rate was excessive; proper annealing conditions resulted in stiff and complete nanowires. Residual AAO helped to maintain the integrity of the molten alloys.

Figure 6.3 (a) TEM image of well-annealed Bi-Sn eutectic nanowires. (b) EDS was used to

determine the composition of nanowires. Mo and Ta peaks arose from TEM grid and heating holder, respectively.

Figure 6.4 CL spectrum of  $\text{BiO}_x\text{-SnO}_x$  nanowires with an average diameter of 70 nm. The curve comprised two emissions - band gap of  $\text{Bi}_2\text{O}_3$  and oxygen vacancies in  $\text{SnO}_2$ .

Figure 6.5 Photoresponse of  $\text{Bi}_2\text{O}_3\text{-SnO}_2$  nanotubes with periodic irradiation at 325 nm in air at bias voltage of 0.8 V.

